POLITECNICO DI TORINO
Repository ISTITUZIONALE

Capturing urban scaling laws via spatio-temporal correlated clusters

Original
Capturing urban scaling laws via spatio-temporal correlated clusters / Carbone, A., da Silva, S.L., Kaniadakis, G. - In: Urban Scaling: Allometry in Urban Studies and Spatial Science / D'Acci, L.. - ELETTRONICO. - [s.l] : Taylor and Francis, 2024. - ISBN 9781003288312. - pp. 310-323 [10.4324/9781003288312-35]

Availability:
This version is available at: 11583/2995386 since: 2024-12-15T09:42:32Z

Publisher:
Taylor and Francis

Published
DOI:10.4324/9781003288312-35

Terms of use:

This article is made available under terms and conditions as specified in the corresponding bibliographic description in the repository

Publisher copyright

(Article begins on next page)

29 November 2026

Urban Scaling

Allometry in Urban Studies and Spatial Science

Edited by Luca S. D'Acci

First published 2025

ISBN: 978-1-032-26440-0 (hbk)
ISBN: 978-1-032-26441-7 (pbk)
ISBN: 978-1-003-28831-2 (ebk)

31 Capturing urban scaling laws via spatio-temporal correlated clusters

Anna Carbone, Sérgio Luiz da Silva, and Giorgio Kaniadakis

CC-BY-NC-ND

DOI: 10.4324/9781003288312-35

Routledge
Taylor & Francis Group
LONDON AND NEW YORK

31 Capturing urban scaling laws via spatio-temporal correlated clusters[1]

Anna Carbone, Sérgio Luiz da Silva, and Giorgio Kaniadakis

31.1 Introduction

A variety of urban features have been reported to exhibit quite universal behaviour depending on population size N. Scaling laws $Y \sim N^{\beta}$ linking socio-economic and infrastructural features to population size, either with $\beta > 1$ or with $\beta < 1$, imply that a more concentrated population corresponds to better socio-economic performances and less costly infrastructural investments [1–4]. The probability density function (pdf) of the population size follows a power-law of N with an exponent approximately equal to 2 [5,6]. Models of monocentric cities have been proposed where individuals commute from home to a central business district (CBD) and back by private or public transportation in a homogeneous isotropic space [7–10]. In such models, population density shows an exponential dependence on the distance from the CBD. Recently, urban landscapes with distinct multicentric activity centres have been envisioned to emerge as population size increases [11] with the monocentric urban organization stable up to a threshold value N^* when a transition to a multicentric structure takes place characterized by a number of business clusters varying with population size as $C_e = N^{\sigma}$ with $\sigma = \mu/(\mu + 1) < 1$ and $0 < \mu < 1$ depending on the congestion level [12,13].

Overall, the scaling features indicate that urban organizations behave as heterogeneous complex systems. Hence, understanding urban microstructure and its evolution over multiple spatio-temporal scales has become a scientific priority with direct practical implications for the sustainable management of big cities [14–17]. The focus of the scientific community has been increasingly drawn towards urban feature description in terms of pointwise rather than cumulative functions of the population size N. In this scenario, the increasing availability of high-resolution spatio-temporal data (phone, satellites) can contribute to investigating models of urban areas and quantifying related phenomena at the local level.

Statistical physics concepts put forward within the subfield of complex systems science have proved relevant to the description of socio-economic and infrastructural urban systems featured by increasing population size and heterogeneity. The investigation of inter- and intra-urban features in heterogeneous multicentric structures has been carried out in terms of spatio-temporal clustering driven by socio-economic

DOI: 10.4324/9781003288312-35
This chapter has been made available under a CC-BY-NC-ND license.

and/or geographical/infrastructural phenomena. A growing number of studies have been addressed to the application of clustering methods in relation to percolation, fractality, self-similarity, self-organization concepts and their statistical significance in the context of urban modelling [18–37]. The Diffusion Limited Aggregation (DLA) model is among the early attempts to describe urban growth phenomena in terms of only one large fractal cluster with a tree-like dendritic structure developed around the central business district, where additional units are randomly added at the periphery. Models where long-range correlated rather than random clusters add to form the city topology could better suit the real urban organization. A percolation process with long-range correlation and an exponential dependence on the distance from the central business district is proposed in [35,36]. A two-dimensional fractional Brownian field is adopted to model the urban grid infrastructure where a set of long-range correlated clusters is generated according to the approach proposed in Ref. [37]. This method is able to reproduce the heterogeneous self-similar urban structure without requiring the assumption of an exponential distribution of the population density with respect to the city centre. Furthermore, it does not operate via a constant thresholding clustering approach, as it is based on a locally varying average function of the spatial field.

This work aims to provide a brief review focused on the adoption of statistical clustering concepts to quantify complexity features of urban landscapes. Special attention will be paid to how scaling laws emerge from long-range correlated clusters with a specific focus on the works [35–37]. This chapter is organized as follows. In Section 31.2 (*Statistical clustering*) the main concepts of clustering algorithms are briefly recalled. In Section 31.2.1 the main steps of the (*Detrending moving average*) algorithm are presented. In Section 31.3 (*Discussion*), a comparison among the methods is provided and the main outcomes, potential implications, and directions for future work are summarized.

31.2 Statistical clustering

Clustering is becoming increasingly relevant for making sense of large amounts of correlated data, where the main aim is identifying patterns intrinsically emerging in the data (natural clusters) rather than building artificial partitions. Several methods and optimization criteria have been proposed that in turn lead to different classes of clustering algorithms. In general, clustering refers to partitioning a dataset into subsets according to some criterion. Let $X = \{\mathbf{x}_1, ..., \mathbf{x}_n\}$ be a set of n data points. Centre-based clustering operates via a partition $C = \{C_1, ..., C_k\}$ of X into k clusters with corresponding centres $\mathbf{c}_1, ..., \mathbf{c}_k$ and allocating data points according to some optimization criterion. The k-centre, k-median, and k-means methods minimize, respectively, the maximum, the sum, and the sum of squares of distances between $\mathbf{c}_k$ and any data point. Despite extensive interesting applications of centre-based clustering, the method suits convex-shaped clusters and requires prior knowledge of the number of cluster k input parameters. An alternative is offered by density-based clustering, which is not affected by these drawbacks as the clusters are built as varying density areas of some relevant feature of the data surrounded by density

values lower than a threshold. Density-based clusters are usually built as sets of points resulting from the intersection through a density function $\delta(r)$ relevant for the data at a certain density level $\bar{\delta}(r)$ (threshold level). Each intersection generates separate connected regions in the feature space where the probability density is higher than the threshold value (see Figure 31.1). Each region corresponds to a cluster defined over all the data points falling into this region. The threshold $\bar{\delta}(r)$ is usually defined as a constant over the whole data domain. If the threshold density level is too small, several clusters will result in being merged together. If the threshold density level is too large, large clusters will not show up. The choice of the threshold is critical to the cluster region definition. In particular, the assumption of a constant threshold is an issue when the relevant feature is not a constant but varies as a long-range correlated quantity of space and time. Such a situation occurs in many real-world systems and is particularly interesting for urban data (e.g., the population size N).

31.2.1 Detrending moving average algorithm

For the sake of completeness, before discussing the application of the detrending moving average (DMA) algorithm to urban landscapes, the main concepts underlying the algorithm together with the essential analytical relationships will be briefly recalled [39,40]. The DMA can be classified as a density-based clustering method with a position-dependent threshold.

Two-dimensional long-range correlated data, such as those featuring urban landscapes, can be modelled in terms of random fields [41,42]. Interesting classes of models for random fields are the fractional Gaussian noise (fGn) and fractional Brownian motion (fBm). A fractional Brownian field $f_H(r)$ is a scalar function with $r=(x_1,x_2,...,x_d)$ the spatial coordinates, d the dimension of the Euclidean domain. The fractional Gaussian noise (*fGn)* is obtained from the fBm increments $f_H(r+1)-f_H(r)$. The fGn is a stationary process with zero mean and covariance given by:

$$\rho(\lambda)=\frac{\sigma^2}{2}\left[(\lambda+1)^{2H}-2\lambda^{2H}+|\lambda-1|^{2H}\right] \sim H(2H-1)\lambda^{2H-2} \tag{31.1}$$

where $\lambda=(\lambda_1,\lambda_2,...,\lambda_d)$ is the scale factor and $|\lambda|==(\lambda_1^2+\lambda_2^2+\ldots+\lambda_d^2)^{1/2}$. The parameter $H\in[0,1]$ is called the Hurst exponent and is linked to the fractal dimension D_f by the relationship $D_f=d-H$. The above properties indicate that fractional Brownian motion and fractional Gaussian noise exhibit long-range correlation and self-similarity.

According to Refs. [39,40] the density threshold is defined by the moving average function $\tilde{f}_H(r)$, that for a two-dimensional space with $d=2$, $r=(x_1, x_2)$ and $\lambda=(n_1, n_2)$ writes:

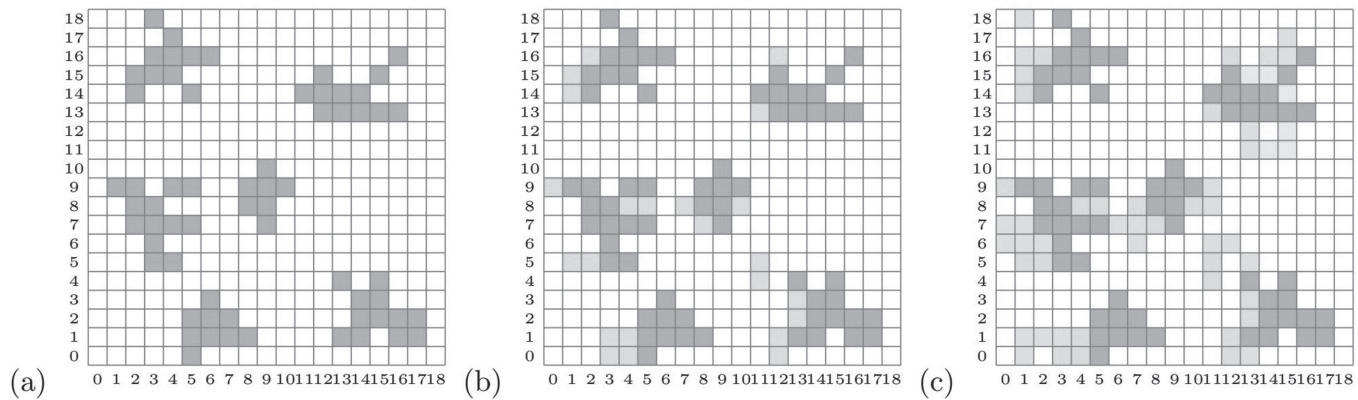


Figure 31.1 Density-based clusters are generated by the intersection between a relevant density function defined at each cell and a threshold. The standard density-based clustering operates with a constant valued threshold. Panels (a), (b), and (c) show how the characteristic size of the clusters scale up as the threshold value decreases. In Refs. [37,38] the threshold is defined as a locally dependent average. The threshold value is determined by the window size $n_1 \times n_2$, which also provides an estimate of the average area of the clusters. In Refs. [35,36] the threshold is a constant.

$$\widetilde{f}_H(x_1,x_2;n_1,n_2)=\frac{1}{n_1n_2}\sum_{k_1=0}^{n_1-1}\sum_{k_2=0}^{n_2-1}f(x_1-k_1,x_2-k_2). \tag{31.2}$$

The function $\widetilde{f}_H(x_1,x_2;n_1,n_2)$ is evaluated at each pair of coordinates x_1, x_2 over sub-arrays with different sizes $n_1 \times n_2$. The clustering is obtained by the intersection of the function $f_H(x_1,x_2)$ with the locally dependent threshold $\widetilde{f}_H(x_1,x_2;n_1,n_2)$ estimated recursively over sub-regions of the grid by varying the values of $n_1 \times n_2$. The difference between the function $f_H(x_1,x_2)-\widetilde{f}_H(x_1,x_2;n_1,n_2)$ generates clusters of increasing area depending on the value of $n_1 \times n_2$.

In Figure 31.2, the function $\widetilde{f}_H(x_1,x_2;n_1,n_2)$ is plotted for $n_1 \times n_2$ equal to (a) 15 × 15, (b) 25 × 25, and (c) 35 × 35. For a rectangular urban grid with size $N_1 \times N_2$, the coordinates x_1, x_2 correspond to each single cell and $n_1 \times n_2$ corresponds to a cell array, i.e., a rectangular sub-area of the urban grid.

In Refs. [39,40], the generalized two-dimensional variance σ^2_{DMA} of $f_H(x_1,x_2)$ around the moving average function $\widetilde{f}_H(x_1,x_2;n_1,n_2)$ is defined as:

$$\sigma^2_{DMA}(n_1,n_2)=\frac{1}{(N_1-n_{1_{max}})(N_2-n_{2_{max}})}\sum_{x_1=n_1}^{N_1}\sum_{x_2=n_2}^{N_2}\left[f_H(x_1,x_2)-\tilde{U}f_H(x_1,x_2;n_1,n_2)\right]^2, \tag{31.3}$$

which can be rewritten as:

$$\sigma^2_{DMA}(n_1,n_2)\sim\left[\sqrt{n_1^2+n_2^2}\right]^{2H}. \tag{31.4}$$

Eq. (31.4) is again a power-law indicating long-range correlation and self-similarity. Hence a log–log plot of σ^2_{DMA} as a function of the scale $s=n_1^2+n_2^2$ would yield a straight line with slope H.

The procedure can be applied to real-world two-dimensional data as for example done in Refs. [37,38]. The scaling behaviour of the DMA method (Eq. 31.4) when implemented on real data as the urban landscape satellite images provides the Hurst exponent of the data. Real-world heterogeneous long-range correlated data are not ideal fractional Brownian motions. Therefore, the subscript H is dropped when the method is applied to real-world data, remarking that a-priori data are not ideal fBms. Contrarily to fractional Brownian functions $f_H(r)$ defined to exist at all scales, real-world datasets barely behave as ideal fractals. Being characterized by finite sizes, setting upper and lower limits to the detection of small and large scales, deviations from the ideal scaling behaviour should be expected.

The Hurst exponent H and the fractal dimension D_f of urbanized regions have been estimated by implementing the two-dimensional detrending moving average

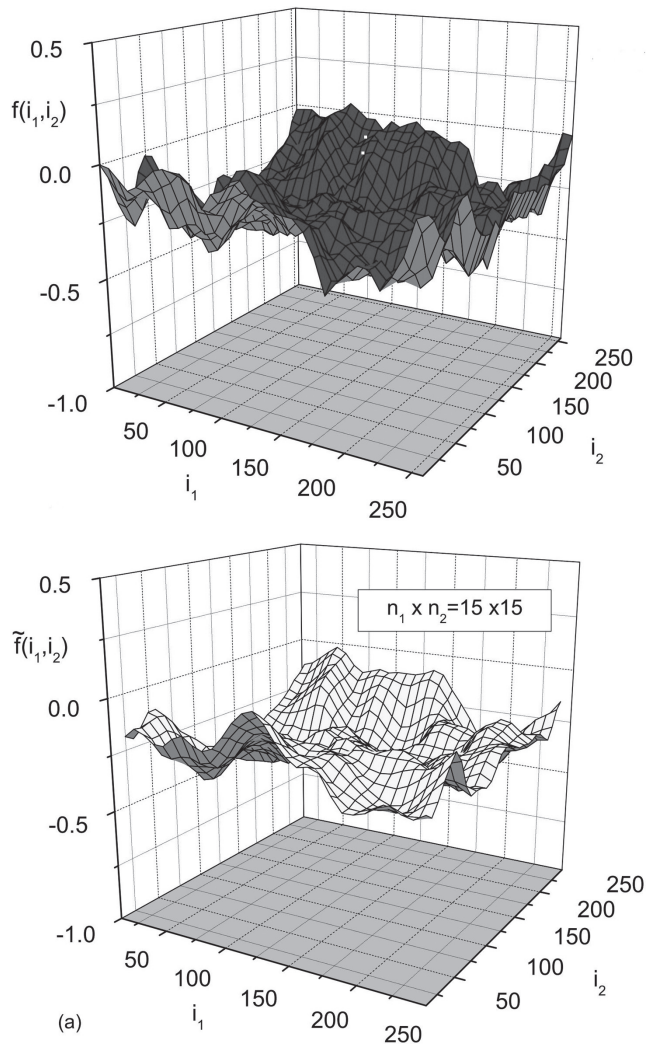


Figure 31.2 Two-dimensional ($d = 2$) Fractional Brownian motion field with $H = 0.5$ (a) and moving averages $\tilde{f}_H(x_1, x_2; n_1, n_2)$ estimated by using Eq. (31.2). The size $n_1 \times n_2$ refers to the local areas over which the moving average is estimated. Values of $n_1 \times n_2$ are (a) 15 × 15, (b) 25 × 25, and (c) 35 × 35.

(DMA) algorithm on satellite images in Refs. [37,38]. The purpose of the investigation is twofold: to provide accurate estimates of H and D_f and shed light on the models of interurban and intraurban scaling laws. The analysed urbanized or rural areas are drawn from satellite images. Before implementing the DMA algorithm, raw data are converted from the *unit8* to the *double* format. The algorithm is

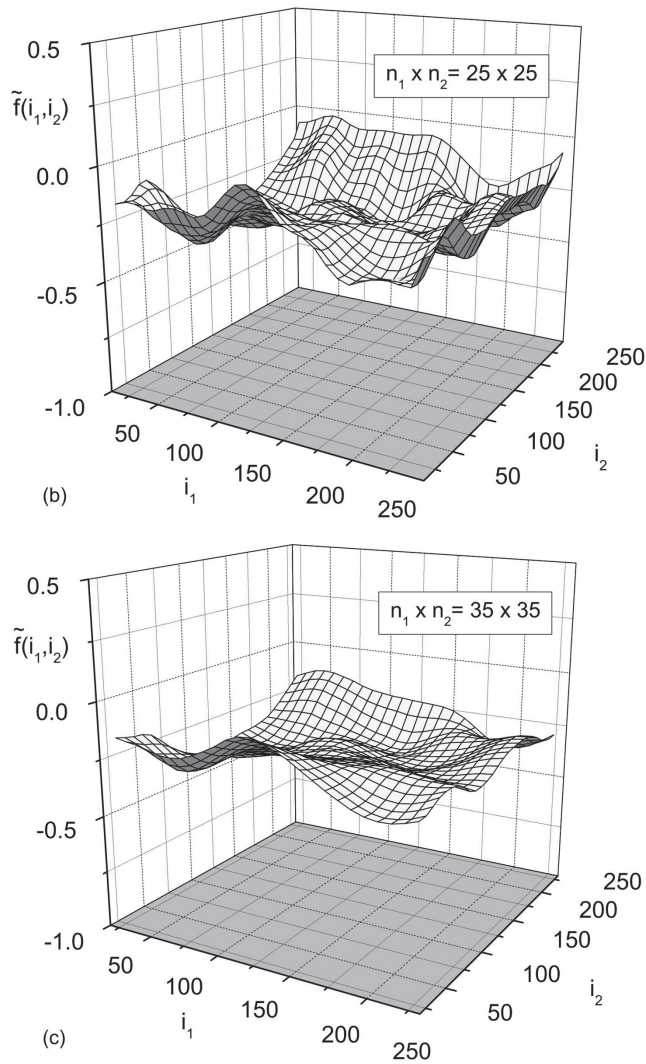


Figure 31.2 Continued

implemented separately on each sub-image, to grasp the variability of the scaling properties of different areas (partially mountainous, suburban, and centrally located areas). Further technical details and results for several intraurban regions of different cities can be found in Ref. [37] and are not repeated here.

The *moving average clustering* optimization criterion can be interpreted as a minimization of an information measure over a partition generated by the threshold $\tilde{f}_H(x_1, x_2; n_1, n_2)$ which is a coarse-grained description of the observed system

obtained by smoothing out the fine details of the real data [43]. As the system becomes coarser, randomness and entropy increase. In the *detrending moving average clustering* threshold $\widetilde{f}_H(x_1, x_2; n_1, n_2)$ is obtained by performing a local average over each cell of the partition in phase space (Figure 31.3).

The difference $f(x_1, x_2) - \widetilde{f}_H(x_1, x_2; n_1, n_2)$ generates a set of regions for each sub-array $n_1 \times n_2$ corresponding to a finite partition $C_{n,j} = \{C_{n,1}, C_{n,2}, ...\}$ of clusters. The difference $f(x_1, x_2) - \widetilde{f}_H(x_1, x_2; n_1, n_2)$ quantifies the error, i.e., the loss of information of the coarse-grained two-dimensional structure compared to the real data. The spatial coordinates (x_1, x_2) where the difference $f(x_1, x_2) - \widetilde{f}_H(x_1, x_2; n_1, n_2)$ becomes zero correspond to the cluster boundaries (Figure 31.4).

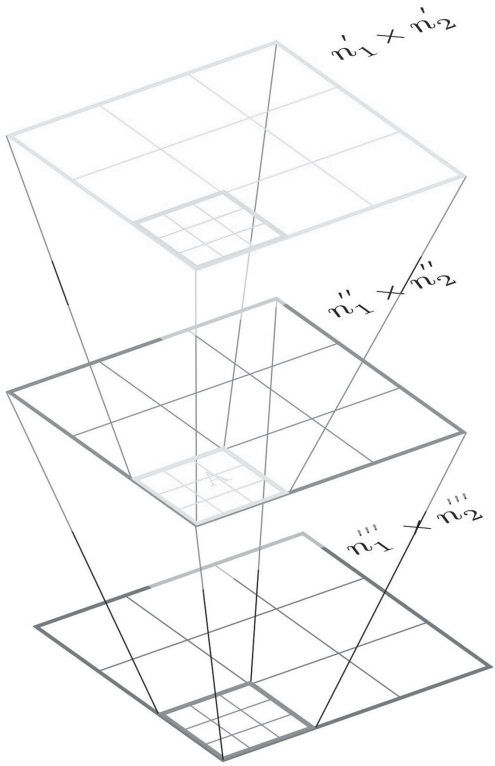


Figure 31.3 The density-based clustering with a non-constant threshold function $\widetilde{f}_H(i_1, i_2; n_1, n_2)$ is adopted in Ref. [37]. The threshold function $\widetilde{f}_H(i_1, i_2; n_1, n_2)$ is defined as a local average and is estimated over a rectangular subset of area $n_1 \times n_2$. The threshold function yields smoother replicas of the original density function as shown in Figure 31.2 where the procedure is implemented on a fractional Brownian motion random field with $H = 0.5$.



Figure 31.4 Image N48-181 (Vienna) of the Urban Atlas of WorldView-2 satellite European Cities collection [44]. The image is multi-spectral with size 1080 × 1080.

31.3 Clustering and scaling laws

The density-based clustering methods of Refs. [35,37] are based on different models: the former adopts percolation, while the latter has a fractional Brownian motion description. Despite this difference, they share the common statistical feature of introducing a two-point long-range correlation among urban cells. The

outcome of the two approaches provides the correlation exponent that has been used to estimate the exponent β of the scaling laws. In particular, the correlation exponent is related to exponent of the Gibrat law in Ref. [35], while in Ref. [37] a relationship between the correlation exponent is discussed against the models [45–47]. The main features of the two approaches will be discussed and compared in this section. The cluster construction starts with the identification of a relevant feature corresponding to a discrete function $f(x_1, x_2)$ at each cell (x_1, x_2) of the urban grid. Next a suitable threshold $\bar{f}(x_1, x_2)$ is defined at each cell. A constant threshold $\bar{f}(x_1, x_2) = 0$ is used in Ref. [35], while the procedure Ref. [37] adopts is a locally dependent threshold $\bar{f}(x_1, x_2) = \tilde{f}(x_1, x_2; n_1, n_2)$ defined in Eq. (31.2). The difference between the data and the threshold quantifies the fluctuations of the relevant urban feature as, for example, the pointwise population density. The fluctuations are found to be scale-invariant, obeying a scaling law with a given correlation exponent.

The common assumption is that the clusters are long-range correlated, hence the two-point correlation is expressed by:

$$\left(f\left(x_i, x_j\right) - \bar{f}\left(x_i, x_j\right)\right)\left(f\left(x_{i'}, x_{j'}\right) - \bar{f}\left(x_{i'}, x_{j'}\right)\right) \sim \frac{\Delta^2}{\left|\left(x_i, x_j\right) - \left(x_{i'}, x_{j'}\right)\right|^{\alpha}} \quad (31.5)$$

where $\left(x_i, x_j\right)$ and $\left(x_{i'}, x_{j'}\right)$ denote a pair of cell coordinates of the urban grid and α is the correlation exponent ($0 < \alpha < 2$). For fluctuations modelled as fractional Gaussian noise, as in Ref. [37] the correlation exponent is related to the Hurst exponent H (see Eq. 31.1). The correlation of the relevant urban feature (e.g., the population density) decays as a power-law of the distance between cells, implying long-range scale-free correlations in the clustering process.

According to Ref. [35], a cluster is defined through the following main steps. A populated cell is selected. The cluster is built by adding all nearest-neighbour cells with a population density larger than a constant threshold. The cluster stops growing when there is no neighbouring cell outside the cluster with population density larger than the threshold which is usually set to zero. The population in a cluster N_i is defined as the sum of the population of all the cells within the cluster.

The *continuum* CCA [36] proceeds as in the above case but the cluster stops growing when no cell with population density larger than the threshold is found at a distance smaller than the coarse graining level. For a population growth rate lower than 1, the mean μ and the standard deviation of the populations $\sigma_1(N_i)$ vary according to a scaling law. For large clusters, one has:

$$\sigma_1^2 = \sum_{j,k}^{N_i} \frac{\Delta^2}{\left|\left(x_i, x_j\right) - \left(x_{i'}, x_{j'}\right)\right|^{\alpha}} \to \Delta^2 \frac{N_i}{a^2} \int \frac{r dr\, d\theta}{r^{\alpha}} \approx \Delta^2 \frac{N_i}{a^2} \frac{r^{-\alpha+2}}{(2-\alpha)} \quad (31.6)$$

where a^2 is the area of each cell and r_c the radius of the cluster. Since $r_c \sim N_i a^2$, one can write:

$$\sigma_i^2 \sim N_i^{2-\alpha/2} \tag{31.7}$$

with the exponent $2-\alpha/2$ larger than 1 and smaller than 2 being $0 < \alpha < 2$.

The standard deviation of the population density σ_i^2 can be related to the standard deviation of the growth rate $\sigma_0^2 \sim S_0^{-\beta}$. By using $S_0 = N_i n$, it results in $\beta = \alpha/4$, with $0 < \beta < 1/2$ as $0 < \alpha < 2$. If $\alpha = 0$, the standard deviation of the populations growth rates has no dependence on the population size ($\beta = 0$), as expected by Gibrat's law.

The long-range correlation exponents yield in Ref. [37] have been used to estimate the scaling exponents β of the scaling law $Y \sim N^{\beta}$ proposed in Refs. [45–47]. This comparison is made by expressing the exponent β of the scaling law in terms of the fractal dimension D_f of the urban landscape. The infrastructural and socio-economic features are written as power laws of the population size $Y \sim N^{\beta}$ respectively with exponents $\beta_i < 1$ and $\beta_s > 1$. According to Ref. [45], the scaling law exponents are defined as:

$$\beta_i = 1 - \frac{D_f}{d\left(d + D_f\right)} \text{ and } \beta_s = 1 + \frac{D_f}{d\left(d + D_f\right)} \tag{31.8}$$

that can be rewritten in terms of the long-range correlation exponent by using the relationship $D_f = d - H$. According to Eq. (31.3), the clustering is obtained by the intersection of the density function mapped from the satellite image with the locally dependent threshold estimated recursively over sub-regions of the grid (pixel by pixel) by varying the values of $n_1 \times n_2$. The log–log plot of σ_{DMA}^2 as a function of the scale $s = n_1^2 + n_2^2$ provides the H value.

Acknowledgments

This work received financial support from the TED4LAT project (a WIDERA initiative within the Horizon Europe Programme, Grant Agreement: 101079206).

Note

1 https://iopscience.iop.org/article/10.1088/2632-072X/ac718e

References

[1] Newling, B. E. (1969). The spatial variation of urban population densities. *Geographical Review*, 59(2), 242–252.

[2] Nordbeck, S. (1971). Urban allometric growth. *Geografiska Annaler. Series B, Human Geography*, 53(1), 54–67.

[3] Bettencourt, L. M. A., Lobo, J., Helbing, D., Kühnert, C., & West, G. B. (2007). Growth, innovation, scaling, and the pace of life in cities. *Proceedings of the National Academy of Sciences*, 104(17), 7301–7306.
[4] Rybski, D., Arcaute, E., & Batty, M. (2019). Urban scaling laws. *Environment and Planning B: Urban Analytics and City Science*, 46(9), 1605–1610.
[5] Zipf, G. K. (1949). *Human behavior and the principle of least effort*. Cambridge, MA (USA): Addison Wesley Press.
[6] Gabaix, X. (1999). Zipf's law for cities: An explanation. *Quarterly Journal of Economics*, 114(3), 739–767.
[7] Alonso, W. (1964). *Location and Land Use. Toward a General Theory of Land Rent*. Cambridge (USA): Harward University Press.
[8] Mills, E. S. (1972). *Urban Economics*. Glenview. Scott: Foreman, & Company.
[9] Muth, R. F. (1969). *Cities and Housing: The Spatial Pattern of Urban Residential Land Use*. Chicago and London: The University of Chicago Press.
[10] Brueckner, J. K. (1987). The structure of urban equilibria: a unified treatment of the muth-mills model. *Handbook of Regional and Urban Economics*, 2, 821–845.
[11] Dubin, R. (1991). Commuting patterns and firm decentralization. *Land Economics*, 67(1), 15–29.
[12] Louf, R., & Barthelemy, M. (2013). Modeling the polycentric transition of cities. *Physical Review Letters*, 111(19), 198702.
[13] Louf, R., & Barthelemy, M. (2014). How congestion shapes cities: From mobility patterns to scaling. *Scientific Reports*, 4, 5561.
[14] Cumbers, A., & MacKinnon, D. (2004). Introduction: Clusters in Urban and Regional Development. *Urban Studies*, 41(5–6), 959–969.
[15] Phelps, N. A. (2021). Which city? Grounding contemporary urban theory. *Journal of Planning Literature*, 36(3), 345–357.
[16] Wu, H., Levinson, D., & Sarkar, S. (2019). How transit scaling shapes cities. *Nature Sustainability, Nature*, 2(12), 1142–1148.
[17] Keuschnigg, M., Mutgan, S., & Hedström, P. (2019). Urban scaling and the regional divide. *Science Advances*, 5(1), eaav0042.
[18] Barthelemy, M. (2019). The statistical physics of cities. *Nature Reviews Physics*, 1(6), 406–415.
[19] Reia, S. M., Rao, P. S. C., Barthelemy, M., & Ukkusuri, S. V. (2022). Spatial structure of city population growth. *Nature Communications*, 13(1), 5931.
[20] Lengyel, J., Roux, S. G., Abry, P., Sémécurbe, F., & Jaffard, S. (2022). Local multifractality in urban systems-the case study of housing prices in the greater Paris region. *Journal of Physics: Complexity*, 3(4), 045005.
[21] Portugali, J. (1997). *Self-Organization, Cities, Cognitive Maps and Information Systems*. In: Hirtle, S.C., Frank, A.U. (eds), Spatial Information Theory A Theoretical Basis for GIS. COSIT 1997. Lecture Notes in Computer Science, vol 1329. Berlin, Heidelberg: Springer. https://doi.org/10.1007/3-540-63623-4_59
[22] Rauws, W., Cozzolino, S., & Moroni, S. (2020). Framework rules for self-organizing cities: Introduction. *Environment and Planning B: Urban Analytics and City Science*, 47(2), 195–202.
[23] Delloye, J., Lemoy, R., & Caruso, G. (2020). Alonso and the scaling of urban profiles. *Geographical Analysis*, 52(2), 127–154.
[24] Portugali, J. (2012). *Self-organization and the city*. Berlin, Heidelberg: Springer Science & Business Media. https://doi.org/10.1007/978-3-662-04099-7

[25] Haken, H., & Portugali, J. (2021). Urban Scaling, Urban Regulatory Focus and Their Interrelations. In: Hermann H., Portugali J. (eds), *Synergetic Cities: Information, Steady State and Phase Transition*. Cham: Springer Series in Synergetics. Springer, 199–215. https://doi.org/10.1007/978-3-030-63457-5

[26] Batty, M., & Longley, P. A. (1987). Fractal-based description of urban form. *Environment and Planning B: Planning and Design*, 14(2), 123–134.

[27] Frankhauser, P. (1998). The fractal approach. A new tool for the spatial analysis of urban agglomerations. *Population: An English Selection*, 10(1), 205–240.

[28] Shen, G. (2002). Fractal dimension and fractal growth of urbanized areas. *International Journal of Geographical Information Science*, 16(5), 419–437.

[29] Tannier, C., & Thomas, I. (2013). Defining and characterizing urban boundaries: A fractal analysis of theoretical cities and Belgian cities. *Computers, Environment and Urban System*s, 41, 234–248.

[30] Lemoy, R., & Caruso, G. (2021). Radial analysis and scaling of urban land use. *Scientific Reports*, 11, 22044.

[31] Liang, B., & Weng, Q. (2018). Characterizing urban landscape by using fractal-based texture information. *Photogrammetric Engineering & Remote Sensing*, 84(11), 695–710.

[32] Yakubo, K., Saijo, Y., & Korošak, D. (2014). Superlinear and sublinear urban scaling in geographical networks modeling cities. *Physical Review E*, 90(2), 022803.

[33] Dong, L., Huang, Z., Zhang, J., & Liu, Y. (2020). Understanding the mesoscopic scaling patterns within cities. *Scientific Reports*, 10, 21201.

[34] Altmann, E. G. (2020). Spatial interactions in urban scaling laws. *PLoS One*, 15(12), e0243390.

[35] Rozenfeld, H. D., Rybski, D., Andrade, J. S., Jr, Batty, M., Stanley, H. E., & Makse, H. A. (2008). Laws of population growth. *Proceedings of the National Academy of Sciences of the United States of America*, 105(48), 18702–18707.

[36] Rozenfeld, H. D., Rybski, D., Gabaix, X., & Makse, H. A. (2011). The area and population of cities: New insights from a different perspective on cities. *American Economic Review*, 101(5), 2205–25.

[37] Carbone, A., Murialdo, P., Pieroni, A., & Toxqui-Quitl, C. (2022). Atlas of urban scaling laws. *Journal of Physics: Complexity*, 3(2), 025007.

[38] Valdiviezo-Navarro, J. C., Castro, R., Cristóbal, G., & Carbone, A. (2014). Hurst exponent for fractal characterization of LANDSAT images. In Remote Sensing and Modeling of Ecosystems for Sustainability XI. *International Society for Optics and Photonics*, 9221, 922103.

[39] Carbone, A., Castelli, G., & Stanley, H. E. (2004). Analysis of clusters formed by the moving average of a long-range correlated time series. *Physical Review E*, 69(2), 026105.

[40] Carbone, A. (2007). Algorithm to estimate the Hurst exponent of high-dimensional fractals. *Physical Review E*, 76(5), 056703.

[41] Isichenko, M. B. (1992). Percolation, statistical topography, and transport in random media. *Reviews of Modern Physics*, 64(4), 961.

[42] Hristopulos, D. T. (2020). *Random Fields for Spatial Data Modeling: A Primer for Scientists and Engineers*. Netherlands: Springer.

[43] Carbone, A., & Ponta, L. (2022). Relative cluster entropy for power-law correlated sequences. *SciPost Physics*, 13(3), 076.

[44] Urban Atlas, last visit on 07/2021. The ESA third party mission collection of the largest European urban areas recorded by the WorldView-2 satellite https://tpm-ds.eo.esa.int/ oads/access/collection/WorldView-2.

[45] Bettencourt, L. M. A. (2013). The origins of scaling in cities. *Science*, 340(6139), 1438–1441.

[46] Ribeiro, F. L., Meirelles, J., Ferreira, F. F., & Neto, C. R. (2017). A model of urban scaling laws based on distance dependent interactions. *Royal Society Open Science*, 4(3), 160926.

[47] Molinero, C., & Thurner, S. (2021). How the geometry of cities determines urban scaling laws. *Journal of the Royal Society Interface*, 18(176), 20200705.